New insights into the recent magma dynamics under Campi Flegrei caldera (Italy) from petrological and geochemical evidence

Buono G.[a], Paonita A.[b], Pappalardo L.[a]*, Caliro S.[a], Tramelli A[a]., Chiodini G.[c]

a - Istituto Nazionale di Geofisica e Vulcanologia, Sezione di Napoli Osservatorio Vesuviano, via Diocleziano 328, 80124, Napoli, Italy

b - Istituto Nazionale di Geofisica e Vulcanologia, sezione di Palermo, via U. La Malfa 153, 90146, Palermo, Italy

c - Istituto Nazionale di Geofisica e Vulcanologia, Sezione di Bologna, via D. Creti 12, 40128, Bologna, Italy

corresponding author (lucia.pappalardo@ingv.it)

Abstract

The Campi Flegrei caldera is considered the most dangerous volcano in Europe and is currently in a new phase of unrest (started in 2000 and still ongoing) that has persisted intermittently for several decades (main crisis occurred from 1950-52, 70-72 and 82-84). Here, by combining the petrological and geochemical data collected in recent decades with numerical simulations, we place new constraints on the source(s) of the current dynamics of the volcano. In particular, we show that the measured (N_2-He-CO_2) geochemical changes at the fumaroles of Solfatara hydrothermal site are the result of massive (about 3 km^3) magma degassing in the deep portion (≥ 200 MPa, 8 km of depth) of the plumbing system. This degassing mechanism would be able to flood the overlying hydrothermal system with hot gas, thus heating and fracturing the upper crust inducing shallow seismicity and deformation. This implies that the deep magma transfer process (≥8 km) has been decoupled from the source of deformation and seismicity, localized in the first kilometers (0-4 km) of caldera-filling rocks. This information on magma transfer depth can have important implications for defining the best monitoring strategies and for forecasting a future eruption.

Finally, this study highlights how petrological and geochemical data allow us to explore the dynamics of the deep portion of the plumbing system and thus trace the occurrence of recharge episodes, in a portion of the ductile lower crust where magma transfer occurs in the absence of earthquakes.

Plain Language Summary

Calderas are volcanic depressions formed as the ground collapses during huge volcanic eruptions. They often exhibit pronounced unrest, with frequent earthquakes, ground uplift, and considerable heat

This article has been accepted for publication and undergone full peer review but has not been through the copyediting, typesetting, pagination and proofreading process, which may lead to differences between this version and the Version of Record. Please cite this article as doi: 10.1029/2021JB023773.

and mass flux that are monitored by volcanologists for eruption forecasting. However, as this activity is due to the complex interactions among magma and hydrothermal system stored beneath the volcano, it is always difficult to predict the evolution of the unrest towards critical conditions until to eruption. The Campi Flegrei caldera is among the most dangerous volcanos in Europe and is currently in a new phase of unrest that has lasted for several decades, whose nature (magmatic or not magmatic) has remained unclear. Here, we combine petrological and geochemical observations collected in recent decades with numerical simulations to place new constraints on the source of the recent dynamics of the volcano. In particular, we show that new deep magma has recharged the shallow reservoir beneath the volcano and flooded the overlying hydrothermal system with hot gas; thereby weakening the upper rocks allowing deformation (ground uplift) and fracturing (seismicity). This information is particularly important in the case of high-risk Campi Flegrei caldera, because it can help to improve defense strategies in case of future eruption.

Keywords

Campi Flegrei caldera; magma dynamics; volcanic unrest

1. Introduction

The Campi Flegrei (CF) caldera, located in the metropolitan area of Naples, is considered among the most dangerous volcanoes in Europe, as it has been the source of large-scale explosive eruptions in the last 250 ky (e.g. Albert et al., 2019; De Vivo et al., 2001; Mastrolorenzo et al., 2006, 2008, 2017; Pappalardo et al., 2008). The largest of these events are the two ignimbrite eruptions of the Campanian Ignimbrite (CI, 300 km^3 DRE, 40 ka, Gebauer et al., 2014) and the Neapolitan Yellow Tuff (40 km^3, 14.9 ka, Deino et al., 2004) that caused the collapse of the 12-km-wide Campi Flegrei caldera, figure 1.

In the last 15 ky volcanism has been concentrated in three epochs of recurrent – mostly explosive – monogenetic volcanic activity (e.g. Bevilacqua et al., 2016), separated by long periods of quiescence, producing about 70 eruptions (with variable Volcanic Explosivity Index, VEI, spanning from 0 to 5). The first epoch was from ~15.0–10.5 ka and included about 34 explosive eruptions totaling ~4.2 km^3; the second epoch was from ~9.6 to 9.1 ka with six explosive eruptions totaling ~0.69 km^3; the third epoch from ~5.5 to 3.8 ka included 16 explosive eruptions and four effusive eruptions totaling ~2.6 km^3 (e.g. Smith et al., 2011). The last eruption (Monte Nuovo, VEI 2, 0.025 km^3) occurred in 1538 AD and was preceded by intense and long-term precursory phenomena (e.g. Di Vito et al., 2016; Liedl et al., 2019). This eruption followed a period of ca 3000 years of quiescence and it is thought to be the initial phase of a new eruptive caldera cycle (Forni et al., 2018).

Consideration of all available petrological data for Campi Flegrei volcanic products, has suggested the existence of a multi-depth magmatic system (e.g. Pappalardo and Buono, 2021 and references therein), constituted by a shallow (150-200 MPa, corresponding to 6-8 km) felsic (trachyte-phonolite) storage area, recharged by a mafic (trachybasalt-shoshonite) deeper (> 200 MPa) source. These reservoirs, identified by petrological data, possibly represent permanent long-lived storage areas, still present today as indicated by geophysical studies (e.g. Costanzo and Nunziata, 2017; De Natale et al., 2006; Fedi et al., 2018; Zollo et al., 2008). In addition, small-volume shallow intrusions (< 200 MPa) may be generated, followed by either rapid cooling (D'Auria et al., 2015; De Siena et al., 2010) or eruption (e.g. Liedl et al., 2019).

After a long period of subsidence following the last eruption, the caldera showed signs of potential reactivation characterized by episodes of ground uplift, shallow seismicity, significant increase in hydrothermal degassing and changes in fluid-geochemistry. A first inversion of the subsidence occurred between 1950-52 (0.5 m of uplift), followed by the two main bradyseismic crises of 1970-72 and 1982-84 (1.7 and 1.8 m of uplift, respectively), which led to a total net elevation of the ground of about 3.5 m in the central sector of the caldera. A new unrest phase since 2005, prompted the Civil Protection to move the Campi Flegrei volcano from the first ("base" or "green") level to the second ("warning" or "yellow") level of alert since the end of 2012.

In the last decades, large quantities of data have been collected and evaluated in scientific research, however many uncertainties still exist on the nature of the subsurface processes driving the unrest, thus making the caldera-related hazard assessment extremely challenging. Particularly, since 1985, the temperature and chemical composition (H_2O, CO_2, H_2S, Ar, N_2, H_2, CH_4 and CO) of fumarolic gases at the Solfatara hydrothermal site have been systematically recorded. They constitute a unique dataset for the large number of samples, for its continuity (~35 years of observations) and for the homogeneity of the sampling and analytical methods used (Chiodini et al., 2021). This comprehensive dataset documents important geochemical changes in the composition of fumarolic fluids, and provides fundamental information on the nature and evolution of the unrest.

In particular, Caliro et al. (2014) documented a decrease in both the N_2/He and N_2/CO_2 ratios since 1985, paralleled by an increase in He/CO_2 at least up to 2006. The model simulations presented by these authors showed that the degassing of an ascending mafic (trachybasalt-shoshonite) magma and/or mixing between magmatic fluids exsolved at various levels during magma ascent, can explain the measured geochemical data. However, the pressure at which this magma degassing occurred as well as its connection with the preceding (1982-84) phase of ground deformation and seismicity have remained elusive until now. Here, to better constrain the depth and nature of the magmatic fluids source(s), we re-

evaluate and refine the proposed degassing models, also in the light of the geochemical data collected in the last years at fumaroles, and in accordance with the most recent petrological knowledge.

Particularly, we have considered all the available petrological data (melt inclusions, geothermobarometry, phase equilibria experiments) on volcanic products emitted from Campi Flegrei districts in the last 40 ka, and combined with numerical models on magma degassing and crystallization, to better constrain physical and chemical conditions of magma storage and ascent and their possible relationship with the variations of geochemical indicators measured at fumaroles in the last 35 years.

We have demonstrated that the magma depressurization trend, depicted by the large variations of inert gases since 1985, took place in the deep portion of the plumbing system, and is thus decoupled from the source of seismicity and ground deformation, located in the shallow portion of the crust (e.g. Amoruso et al., 2014a, 2014b; Battaglia et al., 2006). In particular, two different sources of magmatic gas have been identified, the deepest one (400 MPa) which fed the fumarolic activity measured immediately after the major 82-84 crisis and the second relatively shallow (200 MPa) which feeds the fumarolic activity during the most recent (from 2000 to today) period of unrest. The liberated hot gas progressively floods the overlying hydrothermal system, justifying the increment of shallow seismicity and deformation. This information is crucial for improving monitoring strategies as well as for eruptions forecasting.

2. Material and methods

Degassing model

We performed magma degassing calculations following the approach by Caliro et al. (2014). These authors applied the open-system magma degassing model developed by Nuccio and Paonita (2001) for H_2O–CO_2–N_2–noble-gas mixtures. The model computes the compositional evolution of the gas phase during decompression of a given silicate melt composition according to the solubilities of the involved gases in that melt. The model uses the saturation surface of mixed H_2O–CO_2 vapors to assess the conditions for gas-phase exsolution from a silicate melt, while inert species are regarded as Henrian components of the system. By solving a set of mass–balance and equilibrium equations for volatiles between gas and melt phases, the model computes the composition of the multicomponent gas phase in equilibrium with the silicate melt at a given pressure, temperature, and total abundances of volatiles in the system. Open-system degassing is simulated by infinitesimal steps of decompression, each one starting from the final conditions of the previous step and removing the excess volatiles with respect to the equilibrium saturation at the final pressure of that step. Required input data include (i) initial composition, temperature and saturation pressure of the melt, (ii) composition of the H_2O–CO_2–N_2–He–Ar gas phase at the initial saturation pressure, and (iii) solubilities of all the involved volatiles. Points (i)

and (ii) will be discussed throughout the explored scenarios in Results section while point (iii) will be detailed below.

Coupled decompression and crystallization

In addition to decompression, in this work the degassing process has been also considered to be caused by fractional crystallization. Removal of crystals in fact concentrates the dissolved volatiles in residual melt, so as to cause their oversaturation and degassing. Mass–balance equations were modified to account for the removal of selected amounts of volatile-free crystals for each step of decompression. The amount of crystallization (then the residual fraction of melt) with respect to decompression was regarded as a free parameter to be changed in the degassing model. This is because we cannot constrain the real cooling rate of the magmas during their ascent toward the surface, and consequently their crystallization degree through decompression. The changes of the melt composition with crystallization were computed by fitting each melt oxide content with respect to the residual fraction of melt by using empirical polynomials, along a liquid descent line starting from trachybasalt, through shoshonite to trachyte. The content of Na_2O in the evolved melts was used to estimate the residual fraction with respect to trachybasalt, this approach being suitable for CF potassic series. Although rough, the described approach allows us to estimate the major compositional variation of the residual melt after each decompression/crystallization step. This is extremely important because the composition greatly affects the solubilities of inert gases and, to a minor extent, those of the major volatiles.

Volatiles solubilities

Caliro et al. (2014) provided a wide discussion on the volatile solubilities to be applied in degassing calculations for CF magmas and here we used their selected values. In the following, we briefly recall the main points of their discussion and add some considerations as new experimental data are available.

The H_2O–CO_2 saturation surface was computed using the model of Papale et al. (2006) for the handled melt compositions. A comparison of the modeled solubilities with those experimentally available for melt compositions falling into/close to the spectrum of CF magmas (Behrens et al., 2009; Fanara et al., 2012, 2015; Lesne et al., 2011a, 2011b; Vetere et al., 2011) produced in fact an acceptable match (see Caliro et al., 2014 for details). Although the experimental solubilities in ultrapotassic phonolitic and leucititic melts (Schanofski et al., 2019) do not fit to Papale et al. (2006) model predictions as concerns CO_2, we did not use such a K-rich liquids in our modeling.

The He and Ar solubilities were computed by using the model of Iacono-Marziano et al. (2010), which computes Henry constant (Kh) of the inert gas as a function of the ionic porosity of the melt (IP) and covers a very wide range of anhydrous silicate melt compositions. The effect of dissolved H_2O was accounted for by the approach of Nuccio and Paonita (2000), known as Extended Ionic Porosity model (EIP), in which IP is theoretically computed in H_2O-bearing melts, and an experimentally calibrated

linear relationship between the computed IP and the inert gas solubility allows calculation of the latter. In the case of He, the relationship was calibrated based on experimental studies of He solubility in H_2O-bearing basalts and rhyolites (Paonita et al., 2000), while for Ar, the calibration only regards an alkali-basalt (Paonita et al., 2012).

Importantly the experiments by Paonita et al. (2012) measured Ar solubility in basaltic melt at pressure up to 215 MPa and $P \approx P_{H2O} + P_{CO2} \gg P_{Ar}$, which turned out to be four times higher in 5 wt% H_2O-bearing basalt melt with respect to the dry melt. More recent investigations by Fabbrizio et al. (2017), which however employed very different conditions ($P_{Ar}>P_{H2O}>P_{CO2}$), observed that an increase of dissolved H_2O up to about 2 wt% (at constant dissolved CO_2 content) did not produce any clear changes of Ar solubility in a basalt at 1 GPa, while a further increase up to 5 wt% was associated by an increase in Ar solubility of 2-3X. At pressure of 3–5 GPa, an increasing H_2O concentration up to 5.3 wt.% and CO_2 concentration up to 0.5 wt%, did not produce any systematic effect in Ar solubility. A comparison of data by Paonita et al. (2012) with those in Fabbrizio et al. (2017) is not appropriate because of the very different experimental conditions, especially related to the Ar abundances (see above). Also, the very high Ar contents in the experiments of Fabbrizio et al. (2017) prevents their use for calibrating the EIP model, as they fail to match the Henrian approximation of infinite dilution computed in the model. Importantly, we however note that this latter condition assumed in the EIP model is that typical of magmatic systems in the lithosphere (Ballantine and Burnard, 2002).

As reviewed by Caliro et al. (2014), experimental studies in basaltic, andesitic and simple synthetic silicate melts demonstrated that nitrogen dissolves as molecular species (N_2) when redox conditions and melt compositions are within the typical ranges of terrestrial magmas. In this condition, N_2 solubility practically matches that of Ar due to the similar size of N_2 molecules and Ar atoms and the very poor interaction with the silicate melt structure (see also Mysen, 2013 for a review). Therefore, models of Ar solubility (as the EIP model) can be confidently used to predict N_2 solubility in CF magmas, according to Caliro et al. (2014). For example, N_2 solubility in basalt computed by using EIP model with Ar as a proxy (~0.05 ppm/0.1MPa), matches very well with estimations achieved by using the very recent model of Bernadou et al. (2021) under oxidizing conditions >IW redox buffer, this latter model being calibrated on the entire available dataset of nitrogen solubility in basalts. Similarly, measured N_2 solubility in haplogranites at 200 MPa and NNO+1 (Li et al., 2015) are reproduced by EIP model very well (~0.4ppm/0.1MPa). Recent solubility data in simple synthetic melts suggest that, even at NNO redox conditions, a fraction of nitrogen can dissolve as NH_2^+ and NH_3 complexes in H_2O-bearing melts at pressures higher than 1 GPa, causing modest increases in solubility, while such dissolution mechanism becomes dominant at reducing conditions (Mysen and Fogel, 2010; Mysen et al. 2008).

However, the pressure and compositional conditions of these experiments are far from those modeled in this study.

3. Results

3.1. Depth and nature of magmatic fluids source(s) at Campi Flegrei caldera

We employed petrological data on past eruptive products representative of the entire volcanic history of Campi Flegrei volcanic district, with the aim to fix initial conditions for numerical simulations of magma degassing. In particular, we used the available melt inclusions data to define the initial volatile concentration of the gas phase at equilibrium with trachybasaltic melts as well as initial pressure conditions; the results have been validated by the other independent petrological data (thermodynamic and phase-equilibria data).

The volcanic products emitted throughout the history of Campi Flegrei caldera range in composition from trachybasalt to trachyphonolite. The most differentiated trachytes-phonolites are by far the dominant erupted magmas during the whole volcanic history of the caldera including also the last Monte Nuovo event (1538 AD), whereas the trachybasalts and shoshonites are rarer, being exclusively erupted during the first (Minopoli and Fondo Riccio eruptions) and second (Pigna San Nicola eruption) epochs of activity by vents located at the caldera border along regional faults (e.g. Pappalardo et al., 2002). Moreover, trachybasaltic-shoshonitic compositions are also represented in Phlegraean volcanic district by the products of Ischia (over the past 3 ka, Molara, Vateliero, Cava Nocelle and Arso shoshonitic-latitic tephras) and Procida (60 ka Fiumicello and 22 ka Solchiaro eruptions) islands. In the following discussion, these mafic compositions will be treated together, as common mantle source and parental mafic magmas have been indicated for alkaline Campanian districts (e.g. Peccerillo, 2020 and references therein).

To place constrains on initial magmatic gas composition and pressure, we reviewed the H_2O-CO_2 contents of melt inclusions trapped in olivine and clinopyroxene crystals of the trachybasaltic-shoshonitic deposits of Campanian volcanic districts (figure 2), in light of the solubility model of Papale et al. (2006). The figure 2c shows that the analyzed melt inclusions, have quite homogeneous trachybasaltic composition, making any compositional effect on H_2O-CO_2 solubility trivial (please see supporting information for further details). These trachybasalt melt inclusions record degassing trends starting from minimum entrapment pressures ranging from >400 to 300 MPa (equivalent to depths of 16-12 km using a density of 2600 kg/m^3) with an equilibrium vapor ranging from 75 to 50 mol% CO_2. In particular, the MI composition of Campi Flegrei mafic melts correspond to a starting depth of 300 MPa with a mean exolved CO_2 value of 60 mol%, while most of them suggest last entrapment pressure of 200 MPa or slightly lower. For comparison, the available felsic (trachytic-phonolitic) melt inclusions

compositions entrapped in feldspars of trachytic deposits, indicating degassing trends starting from shallow pressures (≤ 200 MPa), have been also reported in figure 2b. We point out that these sialic melt inclusions have been shown for comparison in a different (specific for sialic rocks) H_2O–CO_2 saturation curves plot, and are not included in our simulations (see following sections). The reported melt-inclusion-based temperatures are of about 1100-1200 °C for trachybasaltic-shoshonitic melts and of about 950 °C for trachytic melts (references in figure 2 and table 1). These values are consistent with pressures and temperatures calculated using MELTS (Ghiorso and Sack, 1995) thermodynamic approach (e.g. Fowler et al., 2007; Pappalardo and Mastrolorenzo, 2010, 2012; Pappalardo et al., 2004, 2008), geothermobarometry (e.g. Balcone−Boissard et al., 2016; Forni et al., 2018; Masotta et al., 2013; Mollo and Masotta, 2014) as well as phase - equilibrium experiments (e.g. Dolfi and Trigila, 1978; Fabbrizio and Carroll, 2008; Perinelli et al., 2019; Pichavant et al., 2014; Scaillet et al., 2008; Stabile and Carroll, 2020), constrained with data from erupted products and summarized in table 1.

3.2. Simulations of degassing scenarios

In the following, we have performed new numerical simulations of magma degassing by using the starting composition defined on the basis of the trachybasaltic melt inclusions in the previous section. Particularly we have explored the following scenarios: 1) high-pressure decompression-driven degassing (first-boiling), 2) decompression coupled to crystallization degassing (second-boiling) and 3) mixing of fluids derived by magmas coming from different pressures. For all the scenarios, given the complete lack of information on N_2, He, and Ar in the CF magmas, the N_2/He, N_2/CO_2 and Ar/CO_2 ratios in the initial gas phase were considered as adjustable parameters to fit to the fumarolic data by performing a typical inverse modeling approach, the same as done in Caliro et al. (2014).

Scenario 1 - Degassing driven by decompression

The first simulated scenarios consider magma degassing driven by decompression. In detail, our simulations were performed starting from a trachybasaltic magma with a 60 mol% CO_2 initial vapor at an initial pressure of 400 – 300 MPa, as suggested by the average distribution of melt inclusions compositions in figure 2. The isothermal (1200°C), open-system magma degassing of the trachybasalts decompressed from 400-300 has been showed in figure 2d. By comparing figure 2a vs. 2c, it is evident that the wide range of CO_2 concentration in gas phase in equilibrium with CF melt inclusions cannot be explained by a single decompressive degassing paths, as this would involve a large variability in the CO_2/H_2O ratios of the pristine magmas. Thus, we have explored initial starting gas composition ranging up to 75 mol% CO_2. Finally, due to the pressure range indicated by most of the mafic and trachyte MIs of CF (see Sect. 3.1), decompressive paths starting from 200MPa were also explored for a comparison and completeness (figure 2d)..

Results show that the observed geochemical changes at fumaroles can be well described by the open-system magma degassing decompressed from 400-300 to 200 MPa (figure 3a green and blue curves respectively), as well as from shallow depth (200 to 100 MPa, figure 3a, red curve) with a 60 mol%. Along these curves, an amount of degassed CO_2 per mass unit of melt can obviously be computed through the decompression step corresponding to the difference between the highest and the lowest N_2/CO_2 ratio observed in the fumaroles. Following Caliro et al. (2014), if considering the total CO_2 flux at Solfatara (>1800 ton d^{-1}) as being representative of the long-term output from the crater, the time span between the highest and the lowest N_2/CO_2 ratio of the fumaroles allows to achieve a total CO_2 output outgassed by the system. By using this last value, the degassed CO_2 amount per mass unit of melt can be converted into a volume of magma that decompressed and degassed in that time span. As a result of this calculation, we estimate that about 3.1 km^3 of magma would have degassed by decompression from 400-300 to 200 MPa. Shallower degassing process starting from 200 MPa, down to 100 MPa (figure 2d, yellow curve and figure 3a), although fitting data well, would imply unlikely large volume of melt (8 km^3, see Caliro et al., 2014). Similar simulations with higher mol% CO_2 initial vapor (75 mol% CO_2), presented by the more primitive Ischia melt inclusions in figure 2, fail to fit the trends for fumarole data (figure 3b).

Scenario 2 - Decompression coupled to crystallization degassing

The second scenario descends from observing trends in melt inclusions volatile composition. CF melt inclusions close to the 200 MPa isobar show similar entrapment pressure but very variable CO_2 concentration in the gas phase. An evolution towards increasing H_2O content in both melt and gas phase can be explained by crystallization-driven degassing, as showed by the computed paths in figure 2d (red curve). We would specify that we do not intend here to simulate what happened before a single past eruption, but we would like to verify if a similar process, possibly recurrent in the progressive growth of the plumbing system, can justify the gases compositional variations measured in the last decades.

Depending on the extent of crystallization with respect to decompression, the paths display patterns moving from sub-vertical (pure decompression) toward near isobaric when crystallization is dominant. When attempting to explain the melt inclusion pattern at CF, we thus need to envisage processes of decompression plus crystallization (at variable ratios) starting from 400 MPa and 75 mol% of CO_2 in gas phase (see figure 2d, green curves). These paths can in fact explain most of the variability of CF melt inclusions. If we compute these paths in the N_2/He vs. N_2/CO_2 plot, with initial N_2/He and N_2/CO_2 ratios the same as from the scenario 1(figure 4), we observe that the curves would have similar slope to those computed by pure decompression with high (75 mol%) CO_2 initial vapor, thus not accurately fitting the data trend for the fumaroles. It is worthy of note that the N_2/CO_2 ratio, being decreasing during the early degassing, starts to increase at more advanced degassing extents due to the evolution of

the melt composition by crystallization. In fact, while CO_2 is more soluble than N_2 in mafic melts, with melt evolution from shoshonite to trachyte, N_2 solubility increases until becoming higher than CO_2. In this case, N_2 is then progressively enriched in the residual melt with respect to CO_2. We also explored a further scenario dominated by crystallization at 200 MPa with very modest decompression (< 40MPa), as suggested by the near isobaric pattern of several Campi Flegrei trachybasaltic-shoshonitic melt inclusions in figure 2. Starting from 75 mol% of CO_2 in gas phase (as it would be suggested by this trend), it is evident that the crystallization-dominated curve does not capture most of the variation of the fumarole data (figure 4), compared with the pure decompression scenario (figure 3).

Scenario 3 – Mixing with magmatic fluids exsolved at different depths

Alternatively, the observed trend in the fumaroles data could also be explained by a third scenario involving mixing between the gases separated from magmas at two different depths (and hence pressures) along a single degassing-plus-crystallization path. Looking at figure 4, the mixing curve was computed by changing the mixing fraction of the high-pressure M1 source from 0 to 1 with respect to the low-pressure M2 source. In this scenario, the M1 endmember corresponds to the possible initial conditions of pressure and volatile phase composition as explored in the scenario 2 (degassing-plus-crystallization), also including the initial N_2/He and N_2/CO_2. Once a decompression-crystallization path has been computed in figure 4, the M2 endmember can be selected along the decompression path in a way that the mixing curve between M1 and M2 will be the best fit of the fumarole data. Because M1 and M2 are for definition two points along a decompression-plus-crystallization path, we are modeling that gas exsolved at M1 (high pressure) mixes to gases exsolved at M2 (low pressure), the mixing process obviously occurring at pressure lower than M2. Physically, we are envisaging two reservoirs at M1 and M2, with M2 being fed by magma raising and crystallizing from M1.

In this model, the gas exsolved at high depth by a deep mafic magma was the source of gas compositions initially (starting from 1985) measured at fumaroles, while the contribution of a second shallower magmatic fluids source became predominant in the last period. As showed in figure 4, mixing curves can explain the fumarolic data very well. In particular, based on the constraints coming from melt inclusions, the most realistic scenarios predict a deep endmember composed of gases with 75 mol% CO_2 exsolved from a magma at 400 MPa (M1 source in figure 4 and 5) mixed with a a shallow gaseous endmember exsolved at 200 MPa (M2 source in figure 4 and 5), along a decompression plus crystallization ascending path starting from the deeper magma. The decompression/crystallization ratio of the ascending path cannot be defined because the shallow endmember would be always able to fit the fumaroles data when mixed with the deep endmember, even using various ratios (figure 4). Indeed, this type of scenarios would be coherent with the compositions of both melt inclusions and fumarole gases.

4. Discussion and Conclusions

Considering the obtained initial magma pressure conditions and gas composition for trachybasaltic melts, our new numerical simulations show that the geochemical variations observed in inert gases in recent decades are controlled by volatile exsolution during deep dynamics of mafic magmas. In this context, our results suggest that the degassing of mafic magma from a pressure of 400 MPa (16 km) can occur i) through direct decompression-induced recharge of about 3.1 km^3 of melt towards the shallow magma layer (150-200 MPa, 7-8 km) (scenario 1) or ii) mixing of gases exsolved by magmas degassed at different depths along a decompression plus crystallization ascending path (scenario 3).

In order to select what would be the most compatible of the two scenarios, we recall that the volatile contents of the melt inclusions addressed to processes of crystallization in addition to the magma decompression (see above), and only scenario 3 considers the crystallization coupled with ascent, a process that cannot be neglected in the dynamic of the plumbing system, as evidenced by the melt inclusion variability. Furthermore, this last scenario explains the behavior of fumarolic gases composition (N_2 and CO_2) measured since 1982, in lights of the concurrent evolution of the geophysical parameters. In particular, N_2/CO_2 ratio abruptly increased during 1982-84 unrest up to a maximum value in 1985, and then progressively decreased until the present value that is comparable to that shown at the beginning of the crisis of the 1980s (figure 5). Similarly, ground uplift and seismicity also rapidly escalated during 1982-84, although they already reached a peak in 1984, while N_2/CO_2 was still increasing. Subsequently, a subsidence with an average rate of 4 cm/yr and an almost seismic quiet persisted until the 2000, when a small uplift and a seismic swarm was registered by the monitoring network of INGV-OV. A more evident increment in the seismicity and a persistent slow uplift, still ongoing, occurred in 2005-2006.

In the view of our petrological, geochemical and geophysical knowledge of the Campi Flegrei plumbing system, we can speculate from scenario 3 that magma decompression coupled with crystallization in the deep (400 MPa) reservoir would have exsolved massive amounts of deeply-sourced gases starting from 1982-84. These fluids would have migrated through the crust and into the shallow reservoir at 200 MPa.

This reservoir possibly acts as a filter, or rheological barrier, promoting the accumulation of deep-sourced mafic magmas under the chamber floor while allowing for upward gas migration.

The existence of such rheological barrier in presence of a shallow reservoir, that favors magma accumulation and enables time for volatiles to escape, has been postulated for active volcanoes (e.g. Merapi volcano, Costa et al., 2013) and reproduced experimentally (Galetto et al., 2017).

The gases liberated from the ascent magma were therefore able to transit the shallow reservoir, ascend to even shallower depths and progressively accumulate in a very shallow gas reservoir, possibly

driving the 1982-84 deformative and seismic unrest. The presence of such a shallow gas reservoir could be consistent with findings from the inversion of geodetic data, which localize the main source of deformation under Campi Flegrei caldera at a depth of 2-4 km (e.g. Amoruso et al., 2014a, 2014b; Battaglia et al., 2006). Although the process of accumulation and pressure buildup occurred in 1982-84, the signature of this gas source in the fumaroles would have become dominant only in 1985, due to the buffering action of the large hydrothermal system below Solfatara on the fumarolic fluid composition (Chiodini et al 2003). Maximum deformation peaked in 1984 and started to decrease in the following years, suggesting that the gas reservoir was no more fed by the deep fluids. The contribution of the deep gas signature also started to decrease as a consequence of the progressive exhaustion and decompression of the shallow gas reservoir and the system moved toward the fumarolic compositions that preceded the main bradyseismic crisis, when the main gas source was the degassing from magma reservoir at 200 MPa. In this view, the onset of new seismic activity and inflation starting slightly in 2000 and clearly in 2005-2006 could be due to increased degassing from this reservoir, although the possible causal relation with the 1982-84 crisis would remain entirely speculative.

It can be of interest to explore the coherence of the scenario 1 (pure decompression) with the above timing of the deformation and geochemistry variations. In this view, 3.1 km^3 of mafic magma transferred from the deep to the shallow (200MPa) storage level, as obtained by our simulations, would be possibly accommodated in the 30 km^3 melt layer identified by seismic tomography at 7.5 km under the volcano (Zollo et al., 2008). Actually, it has been postulated (Befus and Manga, 2019) that the wide magma chambers characteristic of calderas are able to accommodate large volume of magmas as the presence of exsolved volatiles greatly increases magma compressibility, which may buffer volume changes and suppress ground deformation. If the process was responsible for 1982-84 bradyseism, the one-year delay in the peak of the deep gas signature (the highest N_2/CO_2 values, reached only in 1985) would have been caused by the above-mentioned buffer effect of the hydrothermal system. Nevertheless, the N_2/CO_2 peak in 1985 would be related to the onset of the magma transfer occurring at very high pressure, while the following multi-year decreasing trend in N_2/CO_2 would indicate the progressive magma migration from the deep (400 MPa) to the shallow (200 MPa) portion of the plumbing system. In this case, it would not be clear why the strong positive bradyseism occurred in 1982-84 (when magma virtually started to move at 400 MPa), while progressively coming back in the following years (when magma rise was occurring at shallower pressure). Even in this case we should thus hypothesize a gas accumulation zone at 2-4 km where exsolved fluids from 400 MPa massively accumulated in 1982-84, while the contribution of gases coming from the magma ascending towards the shallower system at 200 MPa was lower in the following years. However, this condition would be very similar to that already envisaged above.

In conclusion, we suggest that the observed (N_2-He-CO_2) geochemical changes at the Solfatara fumaroles during the last decades are compatible with mafic magma recharge supplies in the deep portion of the plumbing system. This recharge mechanism would be able to flood the overlying hydrothermal system with hot gas and thus heating and fracturing the upper crust triggering the unrest phases (e.g. Chiodini et al., 2012, 2015a, 2015b, 2016). In particular, mixing of magmatic gases from two different sources has been identified, the deepest one (400 MPa) which fed the fumarolic activity measured immediately after the major 82-84 crisis and the second relatively shallow (200 MPa) which feeds the fumarolic activity during the most recent (from 2000 to today) period of unrest, Figure 6.

Interestingly, the location and the frequency-magnitude distribution of the seismicity recorded since 1982 in the Campi Flegrei caldera support the hypothesis of a volcano dynamic mostly driven by deep magmatic activity during the 82-84 bradyseismic crisis, and by surface hydrothermal activity during the current unrest (from 2000 up to now).

Several differences can be listed between the 1982-84 and the current bradyseismic crises. In 1982-84, the spatial distribution of the earthquakes was spread on the whole caldera, with two identifiable preferential areas: below Solfatara and off-shore on a NW-SE fault. Also, the depth distribution was wide with earthquakes located between 7 km and the surface with a maximum distribution between 2 and 3 km (D'Auria et al., 2011). The seismicity recorded since 2000 is very shallow and highly concentrated below Solfatara (Tramelli et al., 2021) with a maximum distribution between 1 and 1.5 km. This seismicity covers the vertically elongated volume extending below Solfatara, characterized by low Vp/Vs, high attenuation (Calò and Tramelli, 2018) and low resistivity (Siniscalchi et al., 2019), interpreted as a vapor filled volume where earthquakes are induced by shallow hydrothermal gas injections that increase the pore pressure within a highly fractured volume (Tramelli et al., 2021).

In addition, the analysis of the b-value obtained for the two bradyseismic crises confirm a variation in the stress state of the crust. The b-value measures the proportion between large and small earthquakes and depends inversely on differential stress in the crust (Schorlemmer et al., 2005). The seismicity recorded during the 1982-84 bradyseismic crisis has a mean b-value of 0.7 with an anomalous low value (close to 0.5) in the seismic area extending NW-SE in the Pozzuoli bay (D'Auria et al., 2011). The b-value calculated for the seismicity recorded since 2000 has a mean value of 0.9, but is characterized by an increasing trend passing from a value below 1 before 2019 to a value close to 1.3 in 2020 (Tramelli et al., 2021). These values can be related to different stress regimes, higher, more extended and deeper (nearer to the inferred magma chamber roof) stress in 1982-84 and lower and shallower (next to the geothermal system) stress associated to the current unrest.

Our merged results indicate that the massive magmatic degassing process (about 3 km^3 of magma), which caused the variation in the composition of inert gases measured at fumaroles in recent decades,

took place in the deep part of the plumbing system; this implies that this magma transfer process is independent of the source of the deformation and of the seismicity which is instead localized in the first kilometers of crustal rocks that constitute the caldera filling. This information on magma transfer depth can have important implications for defining the best monitoring strategies and for forecasting eruptions.

Finally, this study highlights how petrological and geochemical data allow us to explore the dynamics of the deep portion of the plumbing system and thus trace the occurrence of recharge episodes, in a portion of the ductile lower crust where magma transfer occurs in the absence of earthquakes.

Declaration of Competing Interest

The authors declare that they have no known competing financial interests or personal relationships that could have appeared to influence the work reported in this paper.

Software Availability Statement

The software associated with this manuscript for the simulation of magma degassing is available on open access Zenodo archive https://zenodo.org/deposit/5940213.

Acknowledgements

This work is part of the INGV research project LOVE-CF (Linking surface Observables to sub-volcanic plumbing-system: a multidisciplinary approach for Eruption forecasting at Campi Flegrei caldera (Italy). Petrological and geochemical data is available through Pappalardo and Buono (2021) and Chiodini et al. (2021).

References

Albert, P.G., Giaccio, B., Isaia, R., Costa, A., Niespolo, E.M., Nomade, S., Pereira, A., Renne, P.R., Hinchliffe, A., Mark, D.F., Brown, R.J., Smith, V.C., 2019. Evidence for a large magnitude eruption from Campi Flegrei caldera (Italy) at 29 ka. Geology 47, 595–599. https://doi.org/10.1130/G45805.1.

Amoruso, A., Crescentini, L., Sabbetta, I., 2014a. Paired deformation sources of the Campi Flegrei caldera (Italy) required by recent (1980–2010) deformation history. Journal of Geophysical Research: Solid Earth 119, 858-879. https://doi.org/10.1002/2013JB010392.

Amoruso, A., Crescentini, L., Sabbetta, I., De Martino, P., Obrizzo, F., Tammaro, U., 2014b. Clues to the cause of the 2011–2013 Campi Flegrei caldera unrest, Italy, from GPS data. Geophysical Research Letters 41, 3081-3088. https://doi.org/10.1002/2014GL059539.

Arienzo, I., Mazzeo, F.C., Moretti, R., Cavallo, A., D'Antonio, M., 2016. Open-system magma evolution and fluid transfer at Campi Flegrei caldera (Southern Italy) during the past 5 ka as revealed by geochemical and isotopic data: the example of the Nisida eruption. Chemical Geology 427, 109–124. https://doi.org/10.1016/j.chemgeo.2016.02.007.

Balcone−Boissard, H., Boudon, G., Cioni, R., Webster, J.D., Zdanowicz, G., Orsi, G., Civetta, L., 2016. Chlorine as a geobarometer for alkaline magmas: Evidence from a systematic study of the eruptions of Mount Somma−Vesuvius. Scientific Reports 6, 21726. https://doi.org/10.1038/srep21726.

Ballentine, C.J., Burnard, G.P., 2002. Production, Release and Transport of Noble Gases in the Continental Crust. Reviews in Mineralogy and Geochemistry 47, 481–538. https://doi.org/10.2138/rmg.2002.47.12.

Battaglia, M., Troise, C., Obrizzo, F., Pingue, F., De Natale, G., 2006. Evidence for fluid migration as the source of deformation at Campi Flegrei caldera (Italy). Geophysical Research Letters 33, L01307. https://doi.org/10.1029/2005GL024904.

Befus, K.S., Manga, M., 2019. Supereruption Quartz Crystals and the Hollow Reentrants. Geology 47, 710–714. https://doi.org/10.1130/G46275.1.

Behrens, H., Misiti, V., Freda, F., Vetere, F., Botcharnikov, R., Scarlato, P., 2009. Solubility of H_2O and CO_2 in ultrapotassic melts at 1200 and 1250 °C and pressure from 50 to 500 MPa. American Mineralogist 94, 105–120. https://doi.org/10.2138/am.2009.2796

Bernadou, F., Gaillard, F., Füri, E., Marrocchi, Y., Slodczyk, A., 2021. Nitrogen solubility in basaltic silicate melt - Implications for degassing processes. Chemical Geology 573, 120192. https://doi.org/10.1016/j.chemgeo.2021.120192.

Bevilacqua, A., Flandoli, F., Neri, A., Isaia, R., Vitale S., 2016. Temporal models for the episodic volcanism of Campi Flegrei caldera (Italy) with uncertainty quantification. Journal of Geophysical Research: Solid Earth 121, 7821–7845. https://doi.org/10.1002/2016JB013171.

Buono, G., Pappalardo, L., Harris, C., Edwards, B.R., Petrosino, P., 2020. Magmatic stoping during caldera forming Pomici di Base eruption (Somma-Vesuvius, Italy) as a fuel of eruption explosivity. Lithos 370–371, 105628. https://doi.org/10.1016/j. lithos.2020.105628.

Caliro, S., Chiodini, G., Paonita, A., 2014. Geochemical evidences of magma dynamics at Campi Flegrei (Italy). Geochimica et Cosmochimica Acta 132, 1–15. https://doi.org/10.1016/j.gca.2014.01.021.

Calò, M., & Tramelli, A. (2018). Anatomy of the Campi Flegrei caldera using enhanced seismic tomography models. Scientific reports, 8(1), 1-12.

Cannatelli, C. Understanding magma evolution at Campi Flegrei (Campania, Italy) volcanic complex using melt inclusions and phase equilibria. Miner Petrol 104, 29–42 (2012). https://doi.org/10.1007/s00710-011-0182-6

Chiodini, G., Todesco, M., Caliro, S., Del Gaudio, C., Macedonio, G., Russo, M., 2003. Magma degassing as a trigger of bradyseismic events: The case of Phlegrean Fields (Italy). Geophysical Research Letters 30, 1434. https://doi.org/10.1029/2002GL016790.

Chiodini, G., Caliro, S., De Martino, P., Avino, R., Gherardi, F., 2012. Early signals of new volcanic unrest at Campi Flegrei caldera? Insights from geochemical data and physical simulations. Geology 40, 943–946. http://dx.doi.org/10.1130/G33251.1.

Chiodini, G., Pappalardo, L., Aiuppa, A., Caliro, S., 2015a. The geological CO_2 degassing history of a long-lived caldera. Geology 43, 767–770. https://doi.org/10.1130/G36905.1.

Chiodini, G., Vandemeulebrouck, J., Caliro, S., D'Auria, L., De Martino, P., Mangiacapra, A., Petrillo, Z., 2015. Evidence of thermal-driven processes triggering the 2005–2014 unrest at Campi Flegrei caldera. Earth and Planetary Science Letters 414, 58–67. https://doi.org/10.1016/j.epsl.2015.01.012.

Chiodini, G., Paonita, A., Aiuppa, A., Costa, A., Caliro, S., De Martino, P., Acocella, V., Vandemeulebrouck, J., 2016. Magmas near the critical degassing pressure drive volcanic unrest towards a critical state. Nature Communications 7, 1–9. https://doi.org/10.1038/ncomms13712.

Chiodini, G., Caliro, S., Avino, R., Bini, G., Giudicepietro, F., De Cesare W., Ricciolino, P., Aiuppa, A., Cardellini, C., Petrillo, Z., Selva, J., Siniscalchi, A., Tripaldi, S., 2021. Hydrothermal pressure-temperature control on CO_2 emissions and seismicity at Campi Flegrei (Italy). Journal of Volcanology and Geothermal Research 414, 107245. https://doi.org/10.1016/j.jvolgeores.2021.107245.

Chouet, B. A. (1996). Long-period volcano seismicity: its source and use in eruption forecasting. Nature, 380(6572), 309-316.

Costa, F., Andreastuti, S., Bouvet de Maisonneuve, C., Pallister, J.S., 2013. Petrological insights into the storage conditions, and magmatic processes that yielded the centennial 2010 Merapi explosive eruption. Journal of Volcanology and Geothermal Research 261, 209-235. https://doi.org/10.1016/j.jvolgeores.2012.12.025.

Costanzo, M.R., Nunziata, C., 2014. Lithospheric V_S models in the Campanian Plain (Italy) by integrating Rayleigh wave dispersion data from noise cross-correlation functions and earthquake recordings. Physics of the Earth and Planetary Interiors 234, 46-59. https://doi.org/10.1016/j.pepi.2014.05.002.

D'Auria, L., Giudicepietro, F., Aquino, I., Borriello, G., Del Gaudio, C., Lo Bascio, D., ... & Ricco, C. (2011). Repeated fluid- transfer episodes as a mechanism for the recent dynamics of Campi Flegrei caldera (1989–2010). Journal of Geophysical Research: Solid Earth, 116(B4).

D'Auria, L., Pepe, S., Castaldo, R., Giudicepietro, F., Macedonio, G., Ricciolino, P., Tizzani, P., Casu, F., Lanari, R., Manzo, M., Martini, M., Sansosti, E., Zinno, I., 2015. Magma injection beneath the urban area of Naples: a new mechanism for the 2012–2013 volcanic unrest at Campi Flegrei caldera. Scientific Reports 5, 13100. http://dx.doi.org/10.1038/srep13100.

Deino, A.L., Orsi, G., de Vita, S., Piochi, M., 2004. The age of the Neapolitan Yellow Tuff caldera-forming eruption (Campi Flegrei caldera - Italy) assessed by $^{40}Ar/^{39}Ar$ dating method. Journal of Volcanology and Geothermal Research 133, 157–170. https://doi.org/10.1016/S0377-0273(03)00396-2.

Del Gaudio, C., Aquino, I., Ricciardi, G.P., Ricco, C., Scandone, R., 2010. Unrest episodes at Campi Flegrei: a reconstruction of vertical ground movements during 1905–2009. Journal of Volcanology and Geothermal Research 195, 48–56. http://dx.doi.org/10.1016/j.jvolgeores.2010.05.014.

De Natale, G., Troise, C., Pingue, F., Mastrolorenzo, G., Pappalardo, L., Battaglia, M., Boschi, E., 2006. The Campi Flegrei caldera: unrest mechanisms and hazards. Geological Society, London, Special Publications 269, 25–45. https://doi.org/10.1144/gsl.sp.2006.269.01.03.

De Siena, L., Del Pezzo, E., Bianco, F., 2010. Seismic attenuation imaging of Campi Flegrei: Evidence of gas reservoirs, hydrothermal basins, and feeding systems Journal of Geophysical Research: Solid Earth 115, B09312. https://doi.org/10.1029/2009JB006938.

De Vivo, B., Rolandi, G., Gans, P.B., Calvert, A., Bohrson, W.A., Spera, F.J., Belkin, H.E., 2001. New constraints on the pyroclastic eruption history of the Campanian volcanic Plain (Italy). Mineralogy and Petrology 73, 47-65. https://doi.org/10.1007/s007100170010.

Di Vito, M.A., Acocella, V., Aiello, G., Barra, D., Battaglia, M., Carandente, A., Del Gaudio, C., De Vita, S., Ricciardi, G.P., Ricco, C., Scandone, R., 2016. Magma transfer at Campi Flegrei caldera (Italy) before the 1538 AD eruption. Scientific Reports 6, 32245. https://doi.org/10.1038/srep32245.

Dolfi, D., Trigila, R., 1978. The role of water in the 1944 Vesuvius eruption. Contributions to Mineralogy and Petrology 67, 297–304. https://doi.org/10.1007/BF00381457.

Esposito, R., Bodnar, R.J., Danyushevsky, L.V., De Vivo, B., Fedele, L., Hunter, J., Lima, A., Shimizu, N., 2011. Volatile evolution of magma associated with the Solchiaro Eruption in the Phlegrean Volcanic District (Italy). Journal of Petrology 52, 2431–2460. https://doi.org/10.1093/petrology/egr051.

Esposito, R., Badescu, K., Steele-MacInnis, M., Cannatelli, C., De Vivo, B., Lima, A., Bodnar, R.J., Manning, C.E., 2018. Magmatic evolution of the Campi Flegrei and Procida volcanic fields, Italy, based on interpretation of data from well-constrained melt inclusions. Earth-Science Reviews 185, 325–356. https://doi.org/10.1016/j.earscirev.2018.06.003.

Fabbrizio, A., Carroll, M.R., 2008. Experimental constraints on the differentiation process and pre-eruptive conditions in the magmatic system of Phlegrean Fields (Naples, Italy). Journal of Volcanology and Geothermal Research 171, 88–102. https://doi.org/10.1016/j.jvolgeores.2007.11.002.

Fabbrizio, A., Bouhifd, M.A., Andrault, D., Bolfan-Casanova, N., Manthilake, G., Laporte, D., 2017. Argon behavior in basaltic melts in presence of a mixed H_2O-CO_2 fluid at upper mantle conditions. Chemical Geology 448, 100–109, http://dx.doi.org/10.1016/j.chemgeo.2016.11.014.

Fanara, S., Botcharnikov, R.E., Adams, F., Palladino, D.M. and Behrens, H., 2012. Solubility of H_2O, CO_2, S and Cl in trachytic and trachybasaltic melts of Campi Flegrei (Italy): implications for magma storage conditions. Proc. Cities Volcan., 7.

Fanara, S., Botcharnikov, R.E., Palladino, D.M., Adams, F., Buddensieck, J., Mulch, A., Behrens, H., 2015. Volatiles in magmas related to the Campanian ignimbrite eruption: experiments vs. natural findings. American Mineralogist 100, 2284–2297. https://doi.org/10.2138/am-2015-5033.

Fedi, M., Cella, F., D'Antonio, M., Florio, G., Paoletti, V., Morra, V., 2018. Gravity modeling finds a large magma body in the deep crust below the Gulf of Naples, Italy. Scientific Reports 8, 8229. https://doi.org/10.1038/s41598-018-26346-z.

Forni, F., Degruyter, W., Bachmann, O., De Astis, G., Mollo, S., 2018. Long-term magmatic evolution reveals the beginning of a new caldera cycle at Campi Flegrei. Science Advances 4, eaat9401. https://doi.org/10.1126/sciadv.aat9401.

Fowler, S.J., Spera, F.J., Bohrson, W.A., Belkin, H.E., De Vivo, B., 2007. Phase equilibria constraints on the chemical and physical evolution of the campanian ignimbrite. Journal of Petrology 48, 459–493. https://doi.org/10.1093/petrology/egl068.

Galetto, F., Acocella, V. & Caricchi, L. Caldera resurgence driven by magma viscosity contrasts. Nat Commun 8, 1750 (2017). https://doi.org/10.1038/s41467-017-01632-y.

Gebauer, S.K., Schmitt, A.K., Pappalardo, L., Stockli, D.F., Lovera, O.M., 2014. Crystallization and eruption ages of Breccia Museo (Campi Flegrei caldera, Italy) plutonic clasts and their relation to the Campanian ignimbrite. Contributions to Mineralogy and Petrology 167, 1–18. https://doi.org/10.1007/s00410-013-0953-7.

Ghiorso, M.S., Sack, R.O., 1995. Chemical mass transfer in magmatic processes IV. A revised and internally consistent thermodynamic model for the interpolation and extrapolation of liquid solid equilibria in magmatic systems at elevated temperatures and pressures. Contributions to Mineralogy and Petrology 119, 197–212. https://doi.org/10.1007/BF00307281.

Iacono-Marziano, G., Paonita, A., Rizzo, A., Gaillard, F., Scaillet, B., 2010. Noble gas solubilities in silicate melts: new experimental results and a comprehensive model of the effects of liquid composition,

temperature and pressure. Chemical Geology 279, 145–157. https://doi.org/10.1016/j.chemgeo.2010.10.017.

Lesne, P., Scaillet, B., Pichavant, M., Iacono-Marziano, G., Beny, J., 2011a. The H_2O solubility of alkali basalts: an experimental study. Contributions to Mineralogy and Petrology 162, 133–151. http://dx.doi.org/10.1007/s00410-010-0588-x.

Lesne, P., Scaillet, B., Pichavant, M. and Beny, J., 2011b. The carbon dioxide solubility in alkali basalts: an experimental study. Contributions to Mineralogy and Petrology 162, 163–168. http://dx.doi.org/10.1007/s00410-010-0585-0.

Li, Y., Huang, R., Wiedenbeck, M., Keppler, H., 2015. Nitrogen distribution between aqueous fluids and silicate melts. Earth and Planetary Science Letters 411, 218–228, https://doi.org/10.1016/j.epsl.2014.11.050.

Liedl, A., Buono, G., Lanzafame, G., Dabagov, S.B., Della Ventura, G., Hampai, D., Mancini, L., Marcelli, A., Pappalardo, L., 2019. A 3D imaging textural characterization of pyroclastic products from the 1538 AD Monte Nuovo eruption (Campi Flegrei, Italy). Lithos 340–341, 316–331. https://doi.org/10.1016/j.lithos.2019.05.010.

Mangiacapra, A., Moretti, R., Rutherford, M., Civetta, L., Orsi, G., Papale, P., 2008. The deep magmatic system of the Campi Flegrei caldera (Italy). Geophysical Research Letters 35, L21304. https://doi.org/10.1029/2008GL035550.

Marianelli, P., Métrich, N., Sbrana, A., 1999. Shallow and deep reservoirs involved in magma supply of the 1944 eruption of Vesuvius. Bulletin of Volcanology 61, 48–63. https://doi.org/10.1007/s004450050262.

Marianelli, P., Sbrana, A., Métrich, N., Cecchetti, A., 2005. The deep feeding system Vesuvius involved in recent violent strombolian eruptions. Geophysical Research Letters 32, 1–4. https://doi.org/10.1029/2004GL021667

Marianelli, P., Sbrana, A., Proto, M., 2006. Magma chamber of the Campi Flegrei supervolcano at the time of eruption of the Campanian Ignimbrite. Geology 34, 937–940. https://doi.org/10.1130/G22807A.1.

Masotta, M., Mollo, S., Freda, C., Gaeta, M., Moore, G., 2013. Clinopyroxene‐liquid thermometers and barometers specific to alkaline differentiated magmas. Contributions to Mineralogy and Petrology 166, 1545–1561. https://doi.org/10.1007/s00410‐013‐0927‐9.

Mastrolorenzo G., Pappalardo, L., Troise, C., Rossano, S., Panizza, A., De Natale, G., 2006. Volcanic hazard assessment at the Campi Flegrei caldera. Geological Society, London, Special Publications 269, 159-171. https://doi.org/10.1144/GSL.SP.2006.269.01.10.

Mastrolorenzo, G., Pappalardo, L., Troise, C., Panizza, A., De Natale, G., 2008. Probabilistic tephra hazard maps for the Neapolitan area: Quantitative volcanological study of Campi Flegrei eruptions. Journal of Geophysical Research: Solid Earth 113, B07203. https://doi.org/10.1029/2007JB004954.

Mastrolorenzo, G., Palladino, D. M., Pappalardo, L., Rossano, S., 2017. Probabilistic-numerical assessment of pyroclastic current hazard at Campi Flegrei and Naples city: Multi-VEI scenarios as a tool for "full-scale" risk management. PLOS ONE 12, e0185756. https://doi.org/10.1371/journal.pone.0185756.

Mollo, S., Masotta, M., 2014. Optimizing pre‐eruptive temperature estimates in thermally and chemically zoned magma chambers. Chemical Geology 368, 97–103. https://doi.org/10.1016/j.chemgeo.2014.01.007.

Moretti, R., Arienzo, I., Civetta, L., Orsi, G., D'Antonio, M., 2013. The deep plumbing system of the Ischia island: a physico-chemical window on the fluid-saturated and CO_2-sustained Neapolitan volcanism (Southern Italy). Journal of Petrology 54, 951–984. http://dx.doi.org/10.1093/petrology/egt002.

Mormone, A., Piochi, M., Bellatreccia, F., De Astis, G., Moretti, R., Della Ventura, G., Cavallo, A., Mangiacapra, A., 2011. A CO2 –rich magma source beneath the Phlegraen Volcanic District (Southern Italy): Evidence from a melt inclusion study. Chemical Geology 287, 66–80. https://doi.org/10.1016/j.chemgeo.2011.05.019.

Mysen, B.O., 2013. Structure–property relationships of COHN-saturated silicate melt coexisting with COHN fluid: A review of in-situ, high-temperature, high-pressure experiments Chemical Geology 346, 113–124. https://doi.org/10.1016/j.chemgeo.2012.10.006.

Mysen B.O., Fogel, M.L., 2010. Nitrogen and Hydrogen Isotope compositions and solubility in silicate melts in equilibrium with reduced (N + H)-bearing fluids at high pressure and temperature: effects of melt structure. American Mineralogist 95, 987-999. https://doi.org/10.2138/am.2010.3364.

Mysen, B.O., Yamashita, S., Chertkova, N., 2008. Solubility and solution mechanisms of NOH volatiles in silicate melts at high pressure and temperature – amine groups and hydrogen fugacity. American Mineralogist 93, 1760-1770. https://doi.org/10.2138/am.2008.2879.

Nuccio, P.M., Paonita, A., 2000. Investigation of the He solubility in H_2O–CO_2 bearing silicate liquids at moderate pressure II: the Extended Ionic Porosity (EIP) model. Earth and Planetary Science Letters 183, 499–512. https://doi.org/10.1016/S0012-821X(00)00297-1.

Nuccio P.M., Paonita A., 2001. Magmatic degassing of multicomponent vapors and assessment of magma depth: application to Vulcano Island (Italy). Earth and Planetary Science Letters 193, 467–481. https://doi.org/10.1016/S0012-821X(01)00512-X.

Paonita, A., Gigli, G., Gozzi, D., Nuccio, P.M., Trigila, R., 2000. Investigation of the He solubility in H_2O-CO_2 bearing silicate liquids at moderate pressure: a new experimental method, Earth and Planetary Science Letters 181, 595-604. https://doi.org/10.1016/S0012-821X(00)00215-6.

Paonita, A., Caracausi, A., Iacono-Marziano, G., Martelli, M., Rizzo, A., 2012. Geochemical evidence for mixing between fluids exsolved at different depths in the magmatic system of Mt Etna (Italy). Geochimica et Cosmochimica Acta 84, 380–394. https://doi.org/10.1016/j.gca.2012.01.028.

Papale, P., Moretti, R., Barbato, D., 2006. The compositional dependence of the saturation surface of H_2O + CO_2 fluids in silicate melts. Chemical Geology 229, 78-95. https://doi.org/10.1016/j.chemgeo.2006.01.013.

Pappalardo, L., Buono, G., 2021. Insights Into Processes and Timescales of Magma Storage and Ascent From Textural and Geochemical Investigations, in: Masotta, M., Beier, C., Mollo, S. (Eds.), Crustal Magmatic System Evolution. AGU (American Geophysical Union) Monograph, pp. 213-235. https://doi.org/10.1002/9781119564485.ch10.

Pappalardo, L., Mastrolorenzo, G., 2010. Short residence times for alkaline Vesuvius magmas in a multi - depth supply system: Evidence from geochemical and textural studies. Earth and Planetary Science Letters 296, 133–143. https://doi.org/10.1016/j.epsl.2010.05.010.

Pappalardo, L., Mastrolorenzo, G., 2012. Rapid differentiation in a sill - like magma reservoir: A case study from the campi flegrei caldera. Scientific Reports 2, 712. https://doi.org/10.1038/srep00712.

Pappalardo, L., Piochi, M., D'Antonio, M., Civetta, L., Petrini, R., 2002. Evidence for multi-stage magmatic evolution during the past 60 ka at Campi Flegrei (Italy) deduced from Sr, Nd and P isotope data. Journal of Petrology 43, 1415–1434. https://doi.org/10.1093/petrology/43.8.1415.

Pappalardo, L., Piochi, M., Mastrolorenzo, G., 2004. The 3550 year BP-1944 A.D. magma-plumbing system of Somma-Vesuvius: Constraints on its behaviour and present state through a review of Sr-Nd isotope data. Annals of Geophysics 47, 1471–1483. https://doi.org/10.4401/ag-3354.

Pappalardo, L., Ottolini, L., Mastrolorenzo, G., 2008. The Campanian Ignimbrite (southern Italy) geochemical zoning: Insight on the generation of a super - eruption from catastrophic differentiation and fast withdrawal. Contributions to Mineralogy and Petrology 156, 1–26. https://doi.org/10.1007/s00410 - 007 - 0270 - 0.

Peccerillo, A., 2020. Campania volcanoes: petrology, geochemistry, and geodynamic significance, in: De Vivo, B., Belkin, H.E., Rolandi, G. (Eds.), Vesuvius, Campi Flegrei, and Campanian Volcanism. Elsevier, pp. 79-120. https://doi.org/10.1016/B978-0-12-816454-9.00005-5.

Perinelli, C., Gaeta, M., Bonechi, B., Granati, S.F., Freda, C., D'Antonio, M., Stagno, V., Sicola, S., Romano, C., 2019. Effect of water on the phase relations of primitive K-basalts: implications for high-

pressure differentiation in the Phlegraean Volcanic District magmatic system. Lithos 342, 530e541. https://doi.org/10.1016/j.lithos.2019.05.032.

Pichavant, M., Scaillet, B., Pommier, A., Iacono-Marziano, G., Cioni, R., 2014. Nature an Evolution of Primitive Vesuvius Magmas: an Experimental Study. Journal of Petrology 55, 2281–2310. https://doi.org/10.1093/petrology/egu057.

Scaillet, B., Pichavant, M., Cioni, R., 2008. Upward migration of Vesuvius magma chamber over the past 20,000 years. Nature 455, 216–219. https://doi.org/10.1038/nature07232.

Schanofski, M., Fanara, S., Schmidt, B.C., 2019. CO_2–H_2O solubility in K-rich phonolitic and leucititic melts. Contributions to Mineralogy and Petrology 174, 52. https://doi.org/10.1007/s00410-019-1581-7.

Schorlemmer, D., Wiemer, S., & Wyss, M. (2005). Variations in earthquake-size distribution across different stress regimes. Nature, 437(7058), 539-542.

Siniscalchi, A., Tripaldi, S., Romano, G., Chiodini, G., Improta, L., Petrillo, Z., ... & Avino, R. (2019). Reservoir structure and hydraulic properties of the Campi Flegrei geothermal system inferred by audiomagnetotelluric, geochemical, and seismicity study. Journal of Geophysical Research: Solid Earth, 124(6), 5336-5356.

Smith, V.C., Isaia, R., Pearce, N.J.C., 2011. Tephrostratigraphy and glass compositions of post-15 kyr Campi Flegrei eruptions: implications for eruption history and chronostratigraphic markers. Quaternary Science Reviews 30, 3638–3660. https://doi.org/10.1016/j.quascirev.2011.07.012.

Stabile, P., Carroll, M., 2020. Petrologic experimental data on Vesuvius and Campi Flegrei magmatism: a review, in: De Vivo, B., Belkin, H.E., Rolandi, G. (Eds.), Vesuvius, Campi Flegrei, and Campanian Volcanism. Elsevier, pp. 323-369. https://doi.org/10.1016/B978-0-12-816454-9.00013-4.

Tramelli, A., Godano, C., Ricciolino, P., Giudicepietro, F., Caliro, S., Orazi, M., De Martino, P., Chiodini, G., 2021. Statistics of Seismicity to Investigate the Campi Flegrei Caldera Unrest. Scientific Reports 11, 1. https://doi.org/10.1038/s41598-021-86506-6.

Vetere, F., Botcharnikov, R.E., Holtz, F., Behren, H., De Rosa, R., 2011. Solubility of H_2O and CO_2 in shoshonitic melts at 1250 °C and pressures from 50 to 400 MPa: Implications for Campi Flegrei magmatic systems. Journal of Volcanology and Geothermal Research 202, 251–261. https://doi.org/10.1016/j.jvolgeores.2011.03.002.

Zollo, A., Maercklin, N., Vassallo, M., Dello Iacono, D., Virieux, J., Gasparini, P., 2008. Seismic reflections reveal a massive melt layer feeding Campi Flegrei caldera. Geophysical Research Letters 35, L12306. https://doi.org/10.1029/2008GL034242.

References From the Supporting Information

Cannatelli, C., Lima, A., Bodnar, R.J., De Vivo, B., Webster, J.D., Fedele, L, 2007. Geochemistry of melt inclusions from the Fondo Riccio and Minopoli 1 eruptions at Campi Flegrei (Italy). Chemical Geology 237, 418-432. https://doi.org/10.1016/j.chemgeo.2006.07.012.

Iacovino, K., Matthews, S., Wieser, P.E., Moore, G.M., Bégué, F., 2021. VESIcal Part I: An Open-Source Thermodynamic Model Engine for Mixed Volatile (H_2O-CO_2) Solubility in Silicate Melts. Earth and Space Science 8, e2020EA001584. https://doi.org/10.1029/2020EA001584.

Moore, G., 2008. Interpreting H_2O and CO_2 contents in melt inclusions: constraints from solubility experiments and modeling. Reviews in Mineralogy and Geochemistry 69, 333-361. https://doi.org/10.2138/rmg.2008.69.9.

Papale, P., Moretti, R., Barbato, D., 2006. The compositional dependence of the saturation surface of H_2O+CO_2 fluids in silicate melts. Chemical Geology 229, 78-95. https://doi.org/10.1016/j.chemgeo.2006.01.013.

Captions Figures

Figure 1 – Location map of the Campi Flegrei caldera and Solfatara fumaroles.

Figure 2 – Magmatic gas composition and pressure at Campi Flegrei from melt inclusions data. H_2O–CO_2 saturation curves for trachybasatic (a) and trachytic (b) compositions (according to Papale et al., 2006 at 1200 and 950 °C, respectively). Melt inclusion data (for Phlegraean volcanic district, and Somma-Vesuvius for comparison) are selected from: Marianelli et al. (1999; 2005; 2006), Mangiacapra et al. (2008), Esposito et al. (2011; 2018), Mormone et al. (2011), Moretti et al. (2013), Arienzo et al. (2016). (c) TAS diagram for studied trachybasalt and trachytic-phonolitic melt inclusions (d) Paths of pure decompression-driven degassing and decompression plus crystallization degassing are showed for trachybasalt. High (adv. cryst.), medium (cryst.) and low (soft cryst.) crystallization/decompression ratio of computed corves refer to 0.02, 0.002, and 0.001 crystallized melt fraction/MPa. Paths including crystallization imply an evolution of residual melts towards shoshonite and trachyte. Melt inclusions for Campi Flegrei caldera come from eruptive products of the Astroni, Agnano-Monte Spina (AMS), Campanian Ignimbrite (CI), Fondo Riccio, Minopoli2, Neapolitan Yellow Tuff (NYT), Nisida and Solfatara-Fossa Lupara eruptions.

Figure 3 – Simulated paths of magma degassing by decompression for N_2/He versus N_2/CO_2 ratios. Simulations were performed starting from 60 mol% CO_2 (a) and 75 mol% CO_2 (b) in an initial vapor phase at 400, 300 and 200 MPa, for trachybasalt CF melts. Initial N_2/He and N_2/CO_2 ratios are the same in panel (a) and (b). Squares indicate decompression steps of 100 MPa. Circles display fumarolic data at Solfatara fumaroles (Bocca Grande vent).

Figure 4 - Simulated paths of magma degassing by decompression plus crystallization and by mixing for N_2/He versus N_2/CO_2 ratios. Solid curves describe paths of magma degassing by decompression plus crystallization at variable crystallization/decompression ratios (soft cryst., cryst. and adv. cryst. refer to 0.02, 0.002, and 0.001 crystallized melt fraction/MPa, respectively, see also figure 2; squares indicate decompression steps of 100 MPa). Dotted curves describe mixing of a deep-coming magmatic gas (75 mol% CO_2, 400 MPa) with fluids exsolved at about 180-200 MPa along the given degassing paths. Circles display fumarolic data at Solfatara fumaroles (Bocca Grande vent).

Figure 5 – Time evolution of N_2/He, N_2/CO_2, He/CO_2 (a-c) ratios at Solfatara fumaroles (Bocca Grande vent), and of the elevation (d) at the center of the caldera. Elevation refers to benchmark 25A

(leveling data for 1980-2009, Del Gaudio et al., 2010; GPS data for 2000-2020, station RITE, Tramelli et al., 2021).

Figure 6 - Conceptual model for Campi Flegrei plumbing system (please see text for further explanation).

Table 1 - Intensive variables for Campanian magmas

Methods	**References**	***Composition***	***Pressure***	***Liquidus T***	***Initial water content***
MELTS					
	Fowler et al., 2007	Trachyte	150 MPa	1235 °C	3 wt%
	Pappalardo et al., 2008	Trachyte	250 MPa	1199 °C	4 wt%
	Buono et al., 2020	Trachyte	150 MPa	1160 to ≤ 900 °C	1.62 to ≥ 3 wt%
	Pappalardo & Mastrolorenzo, 2010	Phonolite	250-200 MPa	926 °C	8.6 wt%
	Cannatelli, 2012	Trachyandesite	300-150 MPa		3-2 wt%
	Pappalardo & Mastrolorenzo, 2010	Tephrite	400-350 MPa	1212 °C	5 wt%
	Pappalardo et al., 2014	Tephrite	400 Mpa	1150 °C	saturation
	Buono et al., 2020	Trachybasalt	400 MPa	1240 to 1160 °C	1 to 1.62wt.%
GEOTHERMOBAROMETRY					
cpx-melt thermometers and barometers	Masotta et al., 2013	Trachyte	127-58 MPa	> 884-983 °C	-
cpx-melt thermometry and K-feld-melt hygrometry	Forni et al., 2018	Trachyte	200 MPa	1100 °C	4 wt%
cpx-melt thermometers and barometers	Masotta et al., 2013	Phonolite	157-186 MPa	800-770 °C	-
	Balcone-Boissard et al., 2016	Phonolite	200-180 MPa	-	5.1 wt%
PHASE-EQUILIBRIUM EXP					
	Fabbrizio & Carroll, 2008	Trachyte	200-140 MPa	780°C	saturation condition
	Scaillet et al., 2008	Phonolite	200-100 MPa	815-785 °C	6 wt%
	Pichavant et al., 2014	Trachybasalt	300 - < 200 MPa	1150-1200 °C	1.5-4.5 wt%
	Perinelli et al., 2019	K-basalt	600-900 MPa	1400-1200°C	2 wt%

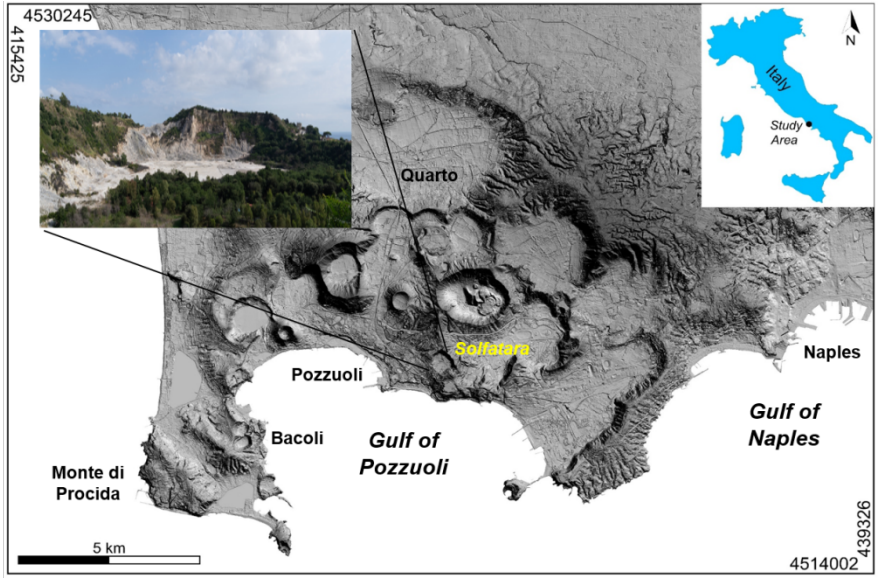
4530245
415425
Quarto
Solfatara
Pozzuoli
Naples
Bacoli
Gulf of Pozzuoli
Gulf of Naples
Monte di Procida
5 km
4514002
439326
N
Italy
Study Area

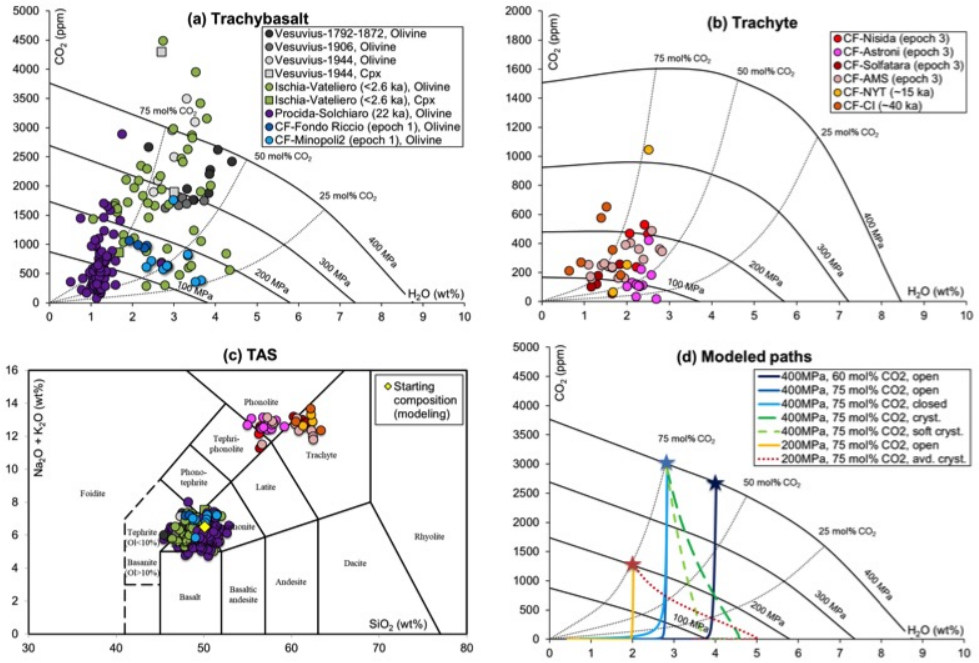

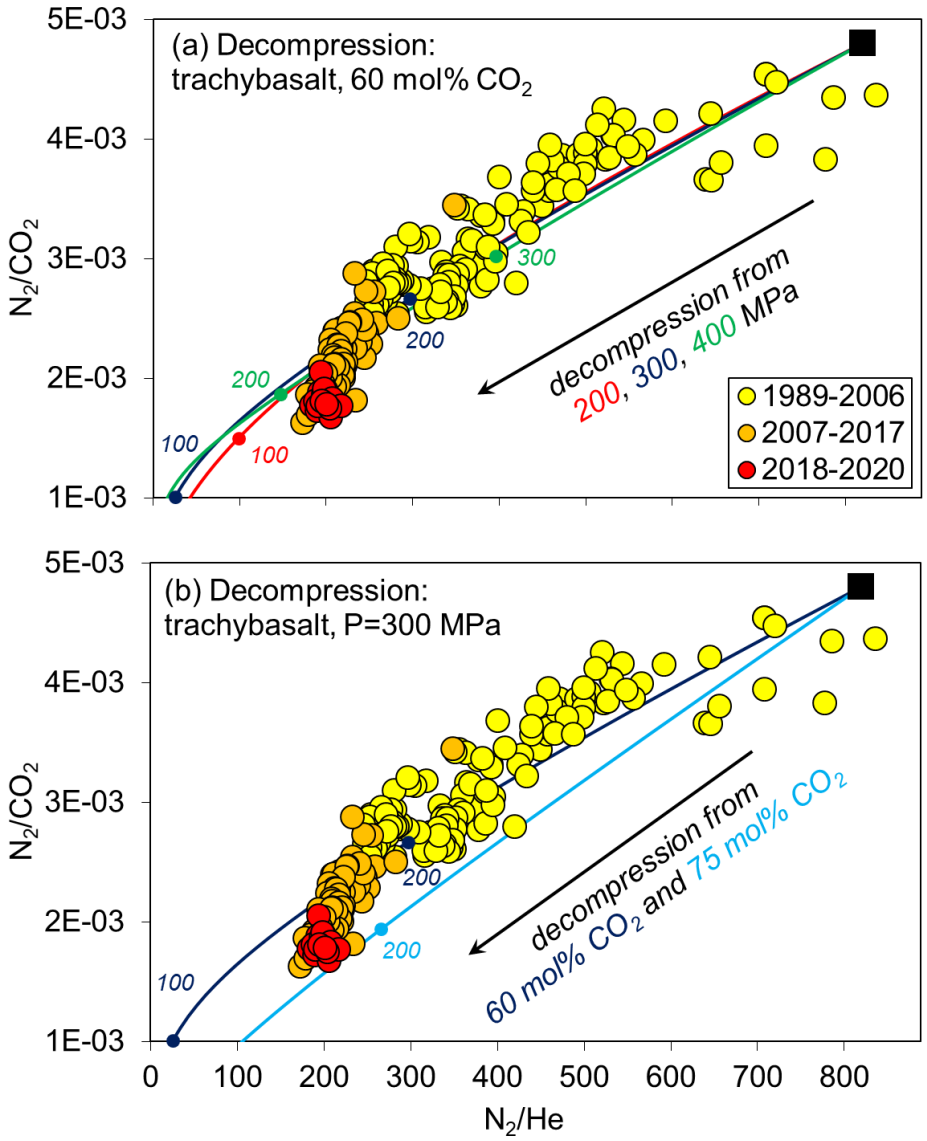
(a) Decompression:
trachybasalt, 60 mol% CO2
5E-03
4E-03
3E-03
2E-03
1E-03
N2/CO2
100
200
300
200
100
decompression from
200, 300, 400 MPa
1989-2006
2007-2017
2018-2020
(b) Decompression:
trachybasalt, P=300 MPa
100
200
200
decompression from
60 mol% CO2 and 75 mol% CO2
0
100
200
300
400
500
600
700
800
N2/He

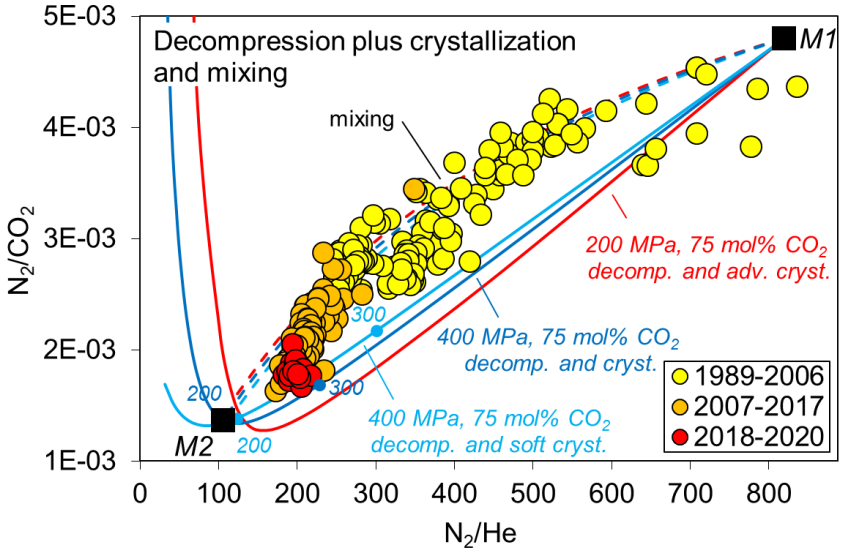
Decompression plus crystallization
and mixing
mixing
M1
M2
200 MPa, 75 mol% CO2
decomp. and adv. cryst.
400 MPa, 75 mol% CO2
decomp. and cryst.
400 MPa, 75 mol% CO2
decomp. and soft cryst.
300
300
200
200
1989-2006
2007-2017
2018-2020
5E-03
4E-03
3E-03
2E-03
1E-03
N2/CO2
0
100
200
300
400
500
600
700
800
N2/He

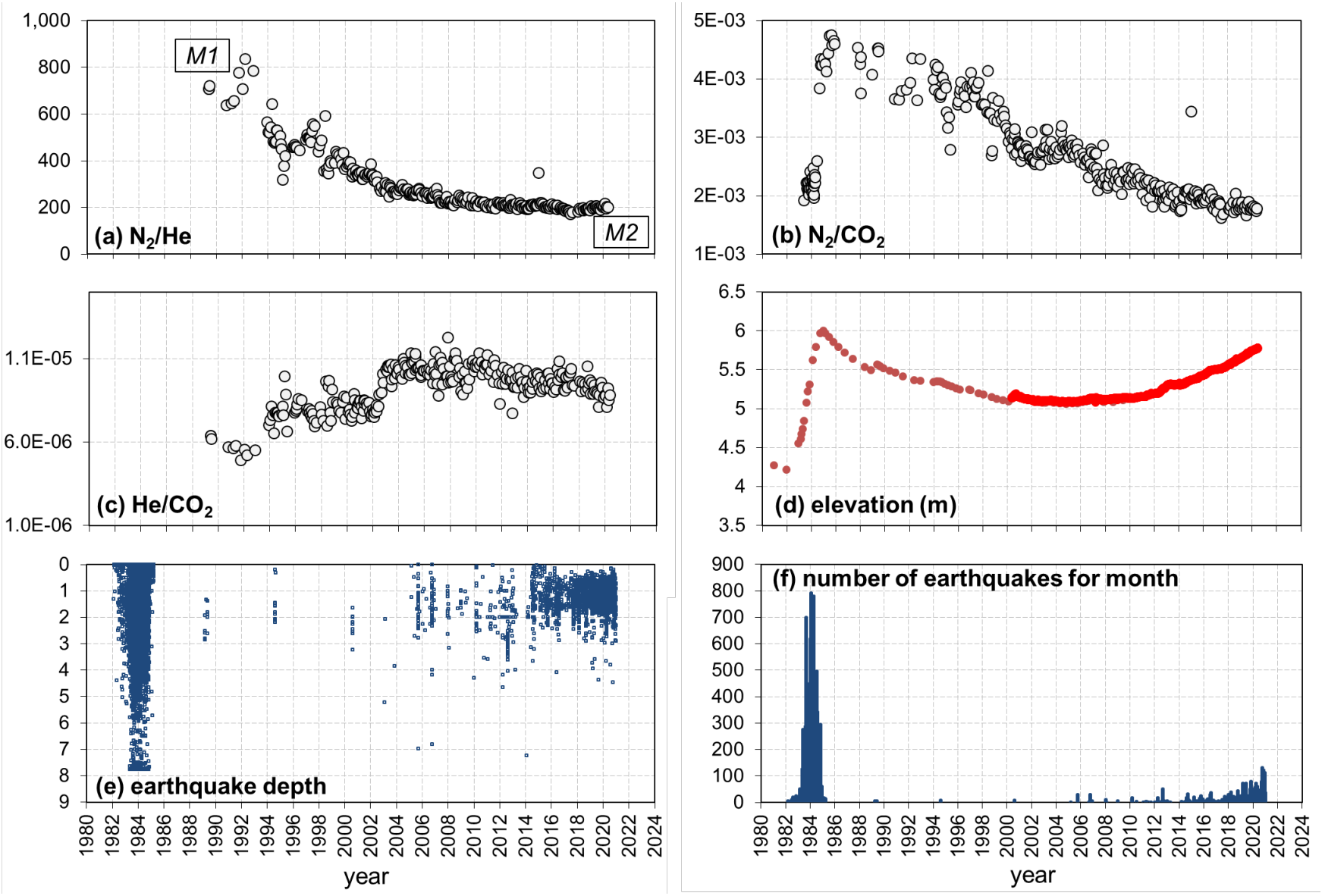
1,000
800
600
400
200
0
M1
M2
(a) N2/He
5E-03
4E-03
3E-03
2E-03
1E-03
(b) N2/CO2
1.1E-05
6.0E-06
1.0E-06
(c) He/CO2
6.5
6
5.5
5
4.5
4
3.5
(d) elevation (m)
0
1
2
3
4
5
6
7
8
9
(e) earthquake depth
900
800
700
600
500
400
300
200
100
0
(f) number of earthquakes for month
1980
1982
1984
1986
1988
1990
1992
1994
1996
1998
2000
2002
2004
2006
2008
2010
2012
2014
2016
2018
2020
2022
2024
year

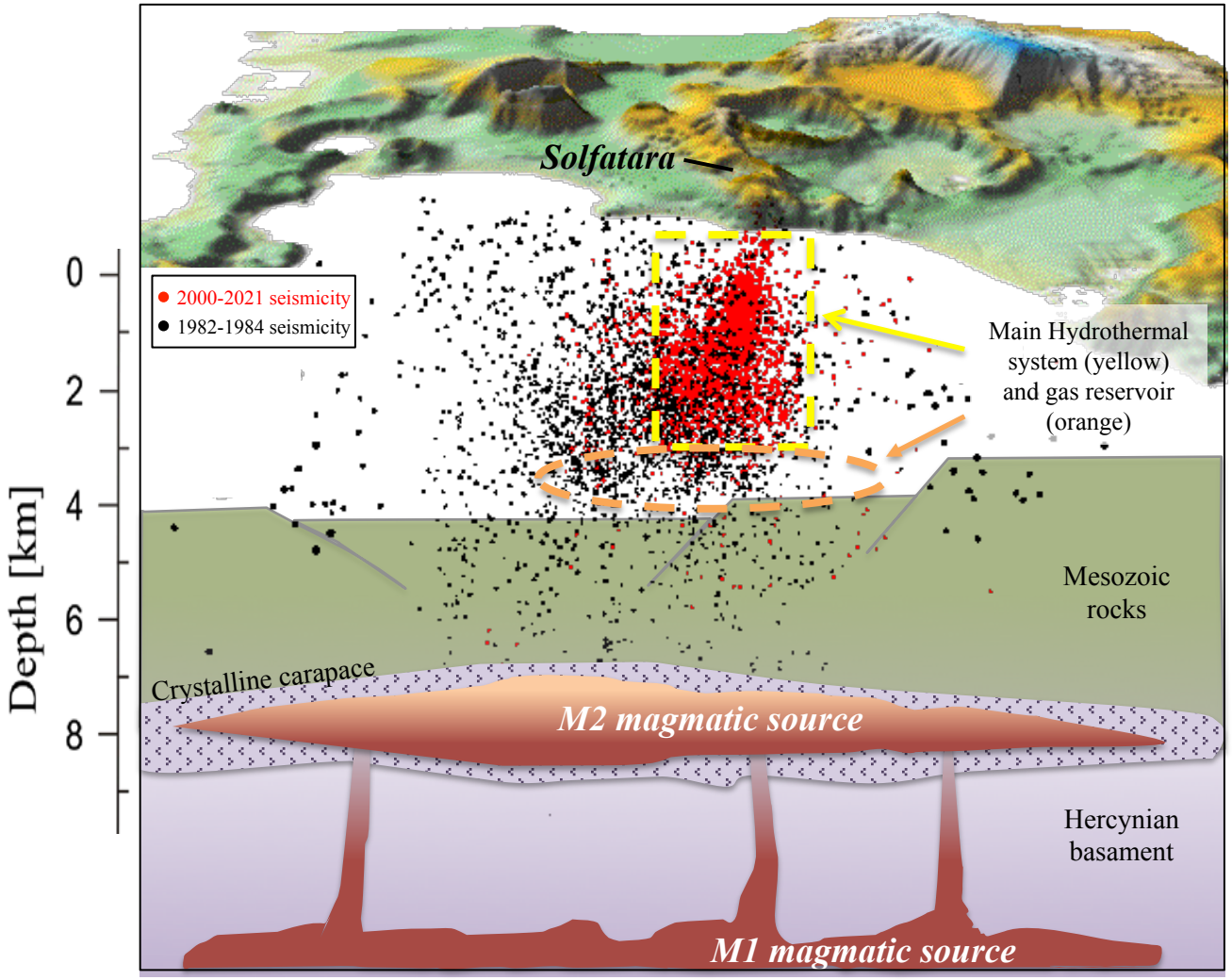
Solfatara
2000-2021 seismicity
1982-1984 seismicity
Main Hydrothermal system (yellow) and gas reservoir (orange)
Depth [km]
0
2
4
6
8
Mesozoic rocks
Crystalline carapace
M2 magmatic source
Hercynian basament
M1 magmatic source